^{61}Ni Mössbauer Effect in Ni-Pd Alloys*

J. E. Tansil† and F. E. Obenshain
Oak Ridge National Laboratory, Oak Ridge, Tennessee 37830
and University of Tennessee, Knoxville, Tennessee 37916

and

G. Czjzek‡
Oak Ridge National Laboratory, Oak Ridge, Tennessee 37830
(Received 22 May 1972)

We have obtained nuclear γ-resonance (NGR) absorption spectra with the 67.4-keV transition from ^{61}Ni in Ni-Pd alloy absorbers throughout the concentration range 0–99.5 at.% Pd. The source contained the parent isotope ^{61}Co, produced by the reaction ^{64}Ni(p, α) ^{61}Co, in a nonmagnetic ^{64}Ni-14 at.% V foil. Both source and absorber were immersed in liquid helium. Values of the absorber recoilless fraction, energy shift, and absolute value of the ^{61}Ni hyperfine (hf) field were obtained for each concentration studied. In the ferromagnetic region 0–98 at.% Pd, the spectra showed a partly resolved magnetic hyperfine splitting with a distribution of magnetic hyperfine fields. The average hyperfine field is negative in pure Ni (−76 kOe), changes sign near 50 at.% Pd, and rises to a large positive value (+173 kOe) at 90 at.% Pd. Qualitative agreement with these results is obtained with a model based on the assumption that $\langle H_{\rm hf}\rangle$ in Ni-Pd has the same contributions from core polarization and bulk conduction-electron polarization as in other Ni-based alloys, *plus* a large positive contribution from Pd atoms on neighboring lattice sites. From measurements with an external magnetic field in alloys containing 50–99.5 at.% Pd, we find that the calculated average hyperfine fields $\langle H_{\rm hf}\rangle_{\rm calc}$ are in agreement with the values expected for no distribution of fields. The distribution width of hyperfine fields is $\Gamma = 80 \pm 9$ kOe in the mid-concentration range. In an alloy containing 0.5 at.% Ni, the most dilute alloy studied, the moment $\mu = [J/(J+1)](0.73 \pm 0.05)\mu_B$ was obtained. From a temperature-dependence study of the second-order Doppler shift, we have deduced the relative isomer shift between ^{61}Ni in Pd and ^{61}Ni in Ni to be $\delta_{\rm IS}^{\rm Pd} - \delta_{\rm IS}^{\rm Ni} = -23 \pm 15$ μ/sec.

I. INTRODUCTION

An experimental study of hyperfine interactions at Ni nuclei in Ni-Pd alloys was undertaken in order to better understand the behavior of ferromagnetic Fe, Co, or Ni alloyed with paramagnetic Pd. These 3*d* transition metals in solution with Pd exhibit ferromagnetism throughout the concentration range, down to solutions as dilute as 0.1% Fe or Co in Pd and 2% Ni in Pd.[1–4] In Fe-Pd and Co-Pd, the moment per 3*d* atom is about $(10–12)\mu_B$ in very dilute solutions but decreases at concentrations as small as 1%,[2,3] whereas in Ni-Pd the moment per Ni atom is about $3\mu_B$ between (2–6)% Ni and decreases at higher concentrations.[3] Neutron scattering experiments have shown that these large moments are related to an induced moment on the Pd atoms by a long-range magnetic interaction.[5] Rather than being spread uniformly throughout the *d* band of the Pd host, the moment per 3*d* atom is local, in the sense that each 3*d* atom, surrounded by polarized Pd neighbors, acts as a single magnetic impurity. Measurements with an external magnetic field on paramagnetic samples of Fe-Pd showed that the hyperfine field of the Fe impurities was consistent with these assumptions.[6]

An understanding of the magnetic properties of the 3*d* alloy systems necessitates the combining of results obtained from many different kinds of experiments: the magnetic moment distribution from neutron scattering; hyperfine fields at the constituent nuclei from nuclear γ-resonance (NGR) spectroscopy, NMR, or perturbed angular correlations; and macroscopic information from saturation magnetization and susceptibility measurements. In the 3*d*-Pd alloys the individual atomic moments have been measured as a function of concentration.[7,8] In Fe-Pd and Co-Pd the moments are, respectively, $\mu_{\rm Fe} \simeq 3\mu_B$ and $\mu_{\rm Co} \simeq 2\mu_B$ and are relatively independent of concentration. On the other hand, the Ni *d* moment increases with increasing Pd content from its pure Ni value of $\mu_{\rm Ni}^d = 0.70\mu_B$ to a maximum of about $1.2\mu_B$ near 90% Pd. Measurements of the hyperfine fields of the alloy constituents have also produced some rather unexpected results. In Table I we give the measured field values for Ni, Co, Fe, and Pd impurities in the same materials as hosts.[9–11] The underlined quantities are relevant to 3*d* Pd alloys. Measurements of the Fe field in Fe-Pd have shown that $\langle H_{\rm hf}^{\rm Fe}\rangle$ remains nearly equal to its value in pure Fe throughout most of the concentration range.[10] However, our measurements[12] and those of Erich *et al.*[13] show that the hyperfine field of Ni in Ni-Pd has an

TABLE I. Hyperfine fields (in kOe) of Fe, Co, Ni and Pd in the same materials as hosts.[a]

		Host			
		Fe	Co	Ni	Pd
Impurity	Fe	−335	−323	−283	−295
	Co	−288	−220	−120	+280
	Ni	−234	−189	−76	+173[b]
	Pd	−594	−400	−194	0

[a]Compiled from Refs. 9–11.
[b]Obtained with a Ni-90% Pd alloy (this work).

entirely different behavior with $\langle H_{hf}^{Ni} \rangle$ increasing from its negative value in pure Ni to a large positive value near the Pd rich end. A similar behavior is observed for the Co field in Co-Pd alloys.[11] These results indicate at least two contributions of opposite sign to the 3*d* hyperfine fields in Co-Pd and Ni-Pd. Although a calculation of the hyperfine field from first principles is beyond the scope of concurrent theoretical models, the principle contributions arise from core polarization, orbital fields, and conduction electron polarization.[14] The major difficulty in correlating the experimental data with theoretical models arises from the cancellation of terms of nearly equal magnitude but opposite sign.

In this paper we give the results of NGR spectroscopy with ^{61}Ni in an investigation of hyperfine interactions at ^{61}Ni nuclei in Ni-Pd alloys throughout the concentration range 0–99.5% Pd. Section II describes the experimental details, including measurements with an external magnetic field and a temperature-dependence study of the second-order Doppler shift. In Sec. III we discuss the interpretation of the applied field results, formulate a model for the alloy magnetism consistent with other available experimental data, and describe the effective-field behavior in the paramagnetic region. The two contributions to the experimental energy shifts, the isomer shift, and the second-order Doppler shift are calculated in Sec. IV.

II. EXPERIMENTAL DETAILS

The technique of NGR spectroscopy with ^{61}Ni employs the 67.4-keV transition from the first excited state to the ground state. The parent isotope ^{61}Co is produced with 22-MeV protons via the reaction ^{64}Ni(p, α) ^{61}Co. The ^{61}Co then undergoes β^- decay to the first excited state of ^{61}Ni. The nonmagnetic sources were 0.1-mm-thick alloy foils of ^{64}Ni-14% V. The properties of the source recoilless-emission spectrum at 4.2 °K were determined from a series of experiments with nonmagnetic Ni-14% V absorbers. The source recoilless fraction was found to be $f_s = (16.2 \pm 0.3\%)$, which can be compared with the recoilless fraction of ^{61}Ni in Ni, $f = 16.4\%$, calculated from neutron inelastic scattering data.[15] The width of the emission line was determined to be $\Gamma_s = 0.42 \pm 0.03$ mm/sec, as compared to the natural linewidth $\Gamma_{nat} = 0.401 \pm 0.016$ mm/sec derived from the measured value of the mean life.[16] Throughout the course of our measurements we observed no effects due to radiation damage in the source.

The Ni-Pd alloy absorbers were manufactured either by arc melting or by induction heating of mixtures of pure Ni and Pd metal powder and then rolling the buttons to thicknesses of 0.1–0.5 mm. All alloys were annealed and then tested for composition and homogeneity with chemical and electron microprobe analyses. Since very small concentrations of Fe and Co in Pd produce magnetic behavior, it was crucial that neither of these magnetic impurities contaminated the dilute Ni in Pd alloys. This was ensured by observing precautions such as rolling the alloy buttons between tantalum foil. Quantitative analyses with a spark-source mass spectrometer on the Ni-Pd alloys containing less than 3% Ni showed that the maximum Fe contamination was 3 ppm and an order of magnitude less for Co.

Most of the details of the NGR spectrometer have been described elsewhere.[17] The data were accumulated in a Nuclear Data 2200 multichannel analyzer (MCA) operated in the time mode. A dual-input option allowed the simultaneous recording of a ^{61}Ni spectrum and an ^{57}Fe calibration spectrum with a one-to-one correspondence between their time scans. The motion of the transducer was correlated with the time scan of the MCA via a square wave originating from the midpoint of the MCA time scan. During repeated cycles of the transducer motion, the data were consecutively stored in one portion of the MCA memory. The velocity scale of the ^{61}Ni spectrum was established by the ^{57}Fe NGR calibration spectrum obtained with a source of ^{57}Co in iron foil, attached to the opposite end of the transducer from the ^{61}Ni source, and an absorber prepared from the same iron foil. An additional feature of the Nuclear Data 2200 analyzer, and a marked improvement over previous models, was a zero-dead-time module which had a pulse-pair resolution of 60 nsec with 30-nsec pulses. This capability completely eliminated analyzer dead time at count rates up to 15 MHz. Thus, the analyzer recycling time between sequential channels was effectively zero and no information was lost due to high counting rates. This was important for many of the ^{61}Ni NGR spectra where count rates in excess of 10^5 counts/sec were encountered.

A glass cryostat (Fig. 1) was used to obtain the zero applied field data at 4.2 °K. Both the source and absorber were immersed in liquid helium. With a source-to-detector distance of 14 cm,

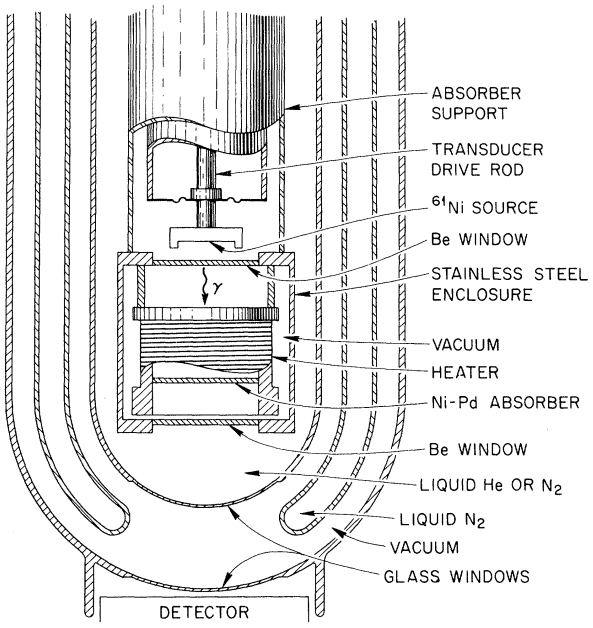

FIG. 1. Cross-sectional view of the bottom part of liquid-helium cryostat used to obtain NGR spectra with $\vec{H}_{ext}=0$ showing the ^{61}Ni γ-ray counting geometry. The absorber heater housing was replaced with a quick-change cartridge holder for experiments at the fixed temperature $T_S=T_A=4.2$ °K.

initial counting rates of typically $(1\text{-}2)\times10^5$ counts/sec were recorded for the 67.4-keV transition from the ^{61}Co sources. Measurements with variable absorber temperature were obtained with the source in liquid nitrogen and the absorber attached to an electrical heater inside an evacuated stainless-steel enclosure. In the range from $T_A=77-300$ °K, the absorber temperature could be maintained to within ±0.5 °K, as monitored with a copper-constantan thermocouple. The measurements which required an external magnetic field parallel to the direction of γ-ray emission along the symmetry axis $\vec{k}$ were obtained with a metal cryostat having a superconducting solenoid capable of fields up to 60 kOe (Fig. 2). Both source and absorber were in the liquid helium with the absorber position at the center plane of the solenoid. Owing to the reduced source-absorber-detector solid angle, initial counting rates were typically 30×10^3 counts/sec, or about one-fourth of the rates obtained with the glass cryostat. The external magnetic field was corrected for demagnetizing field to yield the applied field in the alloy absorber, $H_{ext}-DM$, where $D=4\pi$ is the demagnetizing factor appropriate for a disc and M is the saturation magnetization.[3,18] The magnetic field at the source was always small enough to render corrections for magnetic broadening of the emission line unnecessary.

All of the ^{61}Ni NGR spectra were least-squares fitted to a theoretical line-shape function, the Mössbauer transmission integral,[19] appropriate for a single emission line and a magnetically split absorption line. Relative absorption line intensities were constrained to be equal to the theoretical intensities for both cases $\vec{H}_{ext}=0$ and $\vec{H}_{ext}\parallel\vec{k}$.[20]

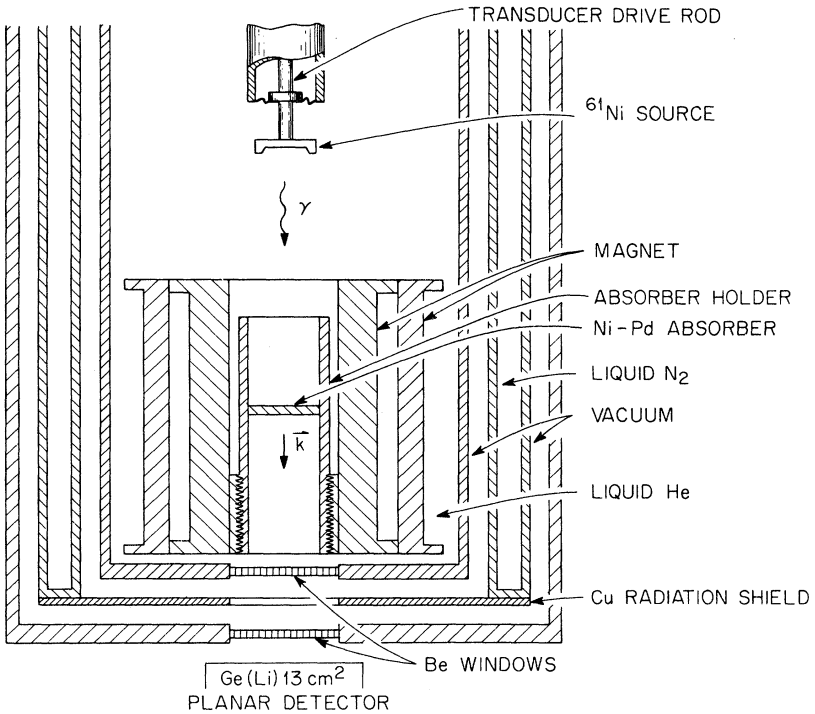

FIG. 2. Cross-sectional view of the bottom part of the liquid-helium cryostat with a superconducting magnet used to obtain NGR spectra with $\vec{H}_{ext}\parallel\vec{k}$.

TABLE II. Parameters of ^{61}Ni NGR absorption spectra of Ni-Pd alloys at 4.2 °K, $H_{ext} = 0$.

Pd conc. (at.%)	^{61}Ni areal density (mg/cm^2)	f_A (%)	δ_{expt} (μ/sec)	$\langle \lvert H_{hf} \rvert \rangle$ (kOe)	$M_2(\lvert H_{hf} \rvert)$ (kOe)^2
0	2.82	16.0±0.6	4±4	75.4±0.3	0
5	2.49	13.8±1.0	1±3	72.7±0.1	20±2
10	2.30	13.4±1.0	0±3	68.4±0.1	43±4
25	1.76	12.9±1.0	5±4	52.5±0.3	131±10
40	1.37	13.2±1.0	14±3	33.8±0.3	192±12
45	4.01	11.1±1.0	15±2	29.2±0.3	125±6
50	3.50	11.0±1.0	23±2	29.9±0.3	92±6
60	3.74	12.4±1.0	21±3	36.8±0.4	295±16
70	3.34	12.6±1.0	26±6	68.0±0.6	641±33
85	3.63	10.8±1.0	28±8	148.6±0.6	567±27
90	4.18	10.3±1.0	24±9	173.2±0.6	379±23
95	3.26	9.0±1.0	31±8	156.4±0.6	264±16
97	3.27	11.9±2.0	32±4	41.9±2.4	...
98	2.35	9.0±0.5	26±4	13.2±0.9	...
98.5	1.69	10.5±0.5	27±3	...	...
99	1.14	10.7±0.5	20±5	...	...
99.5	0.59	7.8±0.5	19±6	...	...

For each spectrum we obtained an energy shift of the resonance centroid and a splitting parameter porportional to the ^{61}Ni effective field. To obtain the correct values for the absorber recoilless fractions at $T = 4.2$ °K, the spectra were scaled for background corrections and count-rate losses due to finite resolving time of the counting electronics.

The spectra obtained in the ferromagnetic region from 0–98% Pd showed a partly resolved magnetic splitting with a considerable broadening of the individual hyperfine component lines. A fitting with the transmission integral, assuming natural linewidth for all lines, is shown in Fig. 3(a) for the alloy Ni-85% Pd. A significantly better fit, Fig. 3(b), was obtained by assuming the line broadening to be caused by a distribution of magnetic fields for a given concentration, and thus nonuniform over the spectrum. The existence of a distribution of fields was fully confirmed by measurements with an external field as described in Sec. III.

III. MAGNETIC HYPERFINE FIELDS AT ^{61}Ni NUCLEI IN Ni-Pd ALLOYS

The parameters derived from ^{61}Ni NGR absorption spectra of Ni-Pd alloys at 4.2 °K are given in Table II. For each alloy we obtained values for the absorber recoilless fraction f_A, energy shift δ_{expt} relative to the ^{64}Ni-V source, hyperfine field $\langle \lvert H_{hf} \rvert \rangle$, and second moment $M_2(\lvert H_{hf} \rvert)$ of the field distribution.

The average field $\langle H_{hf} \rangle$ at ^{61}Ni is negative in pure Ni, changes sign near 50% Pd, and becomes positive for higher Pd concentrations.[12,13] A fact sometimes overlooked is that the magnetic splitting of an NGR spectrum is determined by the absolute field $\lvert H_{hf} \rvert$ irrespective of the sign of $\vec{H}_{hf}$. And since the measurement is an average over all fields, then $\langle \lvert H_{hf} \rvert \rangle$ is the experimentally determined quantity. In the general case of a distribution of magnetic hyperfine fields,

$$\langle \lvert H_{hf} \rvert \rangle \neq \lvert \langle H_{hf} \rangle \rvert \ . \tag{1}$$

Assuming a distribution width Γ, only if $\Gamma \lesssim \lvert \langle H_{hf} \rangle \rvert$ does the relationship become an equality. Usually the hyperfine field is unique (δ-function distribution) and no distinction is made between the two quantities. However, a distribution of fields broadens the sharp hyperfine energy levels, and thus each transition has an energy spread which results in an increase of the individual hyperfine component linewidths. In the region 40–60% Pd, consideration of the relative magnitudes of the line broadening leads to the conclusion that the distribution width Γ will be larger than the average field and the inequality Eq. (1) holds. Hence, in this region an investigation of the effective field at ^{61}Ni as a function of external magnetic field should provide quantitative information about the nature of the distribution. It was also of interest to observe the behavior at other concentrations, particularly in the dilute Ni region where the magnitude of the effective field would give some indication of the size of the moments associated with the Ni impurities in Pd. An external magnetic field was applied to the Ni-Pd absorbers containing 50–99.5% Pd and for each value of the applied field, the effective field and second moment of the distribution were obtained (Table III, Fig. 4).

If the hyperfine field were unique (no distribution of fields), then the effective field as a function of applied field follows the behavior expected for a ferromagnet[21]; thus

$$\vec{H}_{eff} = \vec{H}_{hf} + \vec{H}_{ext} - D\vec{M} \ , \tag{2}$$

where $\vec{H}_{hf}$ is the hyperfine field, $\vec{H}_{ext}$ is the external field, and $D\vec{M}$ is the demagnetizing field. As shown by the dashed lines in Figs. 5(a) and 5(b) for the two alloys Ni-50% Pd and Ni-60% Pd, the effective field will change its magnitude from $\lvert H_{hf} \rvert$ to $\lvert H_{hf} \rvert \pm \lvert (H_{ext} - DM) \rvert$, depending on whether the hyperfine field is parallel or antiparallel to the magnetization. The fact that this behavior was not observed for the two alloys in question arises from the distribution of fields.

An interpretation of the data may be found in the following formulation of the problem. The assumptions are (a) the effective-field model is applicable (spin-spin and spin-lattice interactions do not contribute to the observed broadening), (b) the distribution function $\rho(H)$ is independent of the applied magnetic field H_a [we later choose $\rho(H)$ to be an even function of H, but this is in general not necessary], (c) the magnetic field H is taken to be that

due to a superposition of the magnetic hyperfine interaction field of the electronic states and the Lorentz field,[21] and (d) the quantities determined from our NGR spectra are $\langle|H_{eff}|\rangle$, the average of the absolute value of the effective magnetic field and $M_2(|H_{eff}|)$, the second moment of the field distribution.

Some properties of the distribution are the following: (i) the normalization condition

$$\int_{-\infty}^{\infty}\rho(H)\,dH=1\ ;$$

(ii) the average value of H is

$$\langle H\rangle\equiv\int_{-\infty}^{\infty}H\rho(H)\,dH$$

and the average of the absolute value of H is

$$\langle|H|\rangle\equiv-\int_{-\infty}^{0}H\rho(H)\,dH+\int_{0}^{\infty}H\rho(H)\,dH\ ;$$

(iii) the second moment of H is

$$M_2(H)\equiv\int_{-\infty}^{\infty}H^2\rho(H)\,dH-\langle H\rangle^2$$

and the second moment of $|H|$ is

$$M_2(|H|)\equiv\int_{-\infty}^{\infty}H^2\rho(H)\,dH-\langle|H|\rangle^2\ ;$$

and (iv) the distribution $\rho(H)$ should be nonzero for some range of H including some values for $H<0$. From the definitions of $\langle H\rangle$ and $\langle|H|\rangle$, it follows that

$$\langle|H|\rangle=\langle H\rangle-2\int_{-\infty}^{0}H\rho(H)\,dH=\langle H\rangle-2D\ , \tag{3}$$

where $D\equiv\int_{-\infty}^{0}H\,\rho(H)\,dH$ is a measure of the overlap of the distribution function with the negative H axis.

If the magnetic field is changed by an amount H_a, then the following relations hold:

$$\langle|H+H_a|\rangle=\langle|H|\rangle+H_a+2\int_{-H_a}^{0}H\rho(H)\,dH-2H_a\int_{-\infty}^{-H_a}\rho(H)\,dH \tag{4}$$

and

$$M_2(|H+H_a|)=M_2(|H|)+\langle|H|\rangle^2+2H_a\langle H\rangle-\langle|H+H_a|\rangle^2+H_a^2\ . \tag{5}$$

TABLE III. Effective fields at ^{61}Ni in Ni-Pd alloys (50–99.5% Pd) as a function of external magnetic field.

Pd conc. (at.%)	$H_{eff}-DM$ (kOe)	$\langle\|H_{eff}\|\rangle$ (kOe)	$M_2(\|H_{eff}\|)$ (kOe)^2	$\langle H_{hf}\rangle_{calc}$ (kOe)	$D\equiv\int_{-\infty}^{0}H\,\rho(H)\,dH$ (kOe)
50	0	29.9±0.3	92±6	...	...
	10.0	26.5±0.3	143±10	−12.0	−21±1
	25.0	29.8±0.4	291±14	− 8.6	−19±1
	40.8	37.3±0.4	438±23	−10.2	−20±1
60	0	36.8±0.4	295±16	...	...
	17.5	44.2±0.7	494±35	21.4	− 8±1
	41.2	68.2±0.6	690±35	24.2	− 6±1
70	0	68.0±0.6	641±33	...	...
	41.7	110.1±0.8	759±42	70.5	1±1
85	0	148.6±0.6	567±27	...	...
	43.2	190.4±1.0	759±45	145	2±1
90	0	173.2±0.6	379±23	...	...
	43.8	215.5±1.1	563±48	167	3±2
95	0	156.4±0.6	...	...	...
	44.8	213.4±0.9	...	...	...
97	0	41.9±2.4	...	...	...
	45.8	175.3±1.1	...	...	...
98	0	13.2±0.9	...	...	...
	45.7	139.9±1.0	...	...	...
98.5	0	0	...	...	...
	45.8	117.0±1.0	...	...	...
99	0	0	...	...	...
	45.8	102.4±1.1	...	...	...
99.5	0	0	...	...	...
	15.0	28.0±1.0	...	...	...
	27.6	51.5±1.4	...	...	...
	37.1	72.1±1.7	...	...	...
	45.8	84.0±1.7	...	...	...
	50.3	93.8±1.7	...	...	...

Solving Eq. (5) for $\langle H\rangle$ gives

$$\langle H\rangle = (1/2H_a)[\langle|H+H_a|\rangle^2 - \langle|H|\rangle^2 - H_a^2 + M_2(|H+H_a|) - M_2(|H|)]\,. \quad (6)$$

The overlap integral D then follows from Eq. (3):

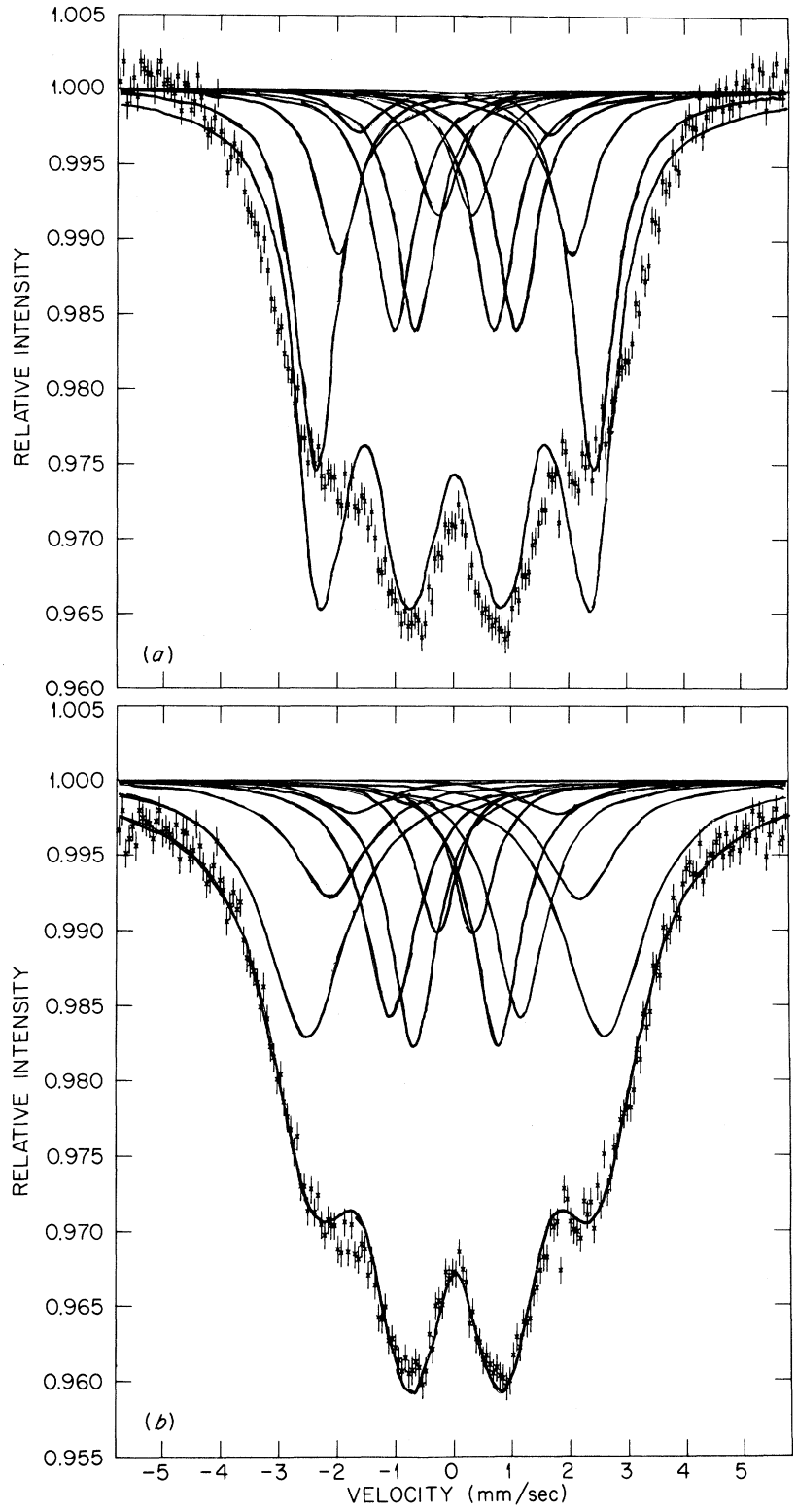

FIG. 3. (a) ^{61}Ni NGR spectrum of Ni-85% Pd at 4.2 °K showing a least-squares fit with the transmission integral assuming natural linewidth for all lines. (b) Fit of the same spectrum with the line broadening assumed to be caused by a distribution of hyperfine fields.

$$D = \tfrac{1}{2}(\langle H \rangle - \langle |H| \rangle) \ . \qquad (7)$$

We now make the obvious identification $H = H_{hf}$ and $H_a = H_{ext} - DM$, where H_{hf} is the ^{61}Ni hyperfine field and H_a is the applied magnetic field. Hence, the average hyperfine field [Eq. (6)] can be calculated

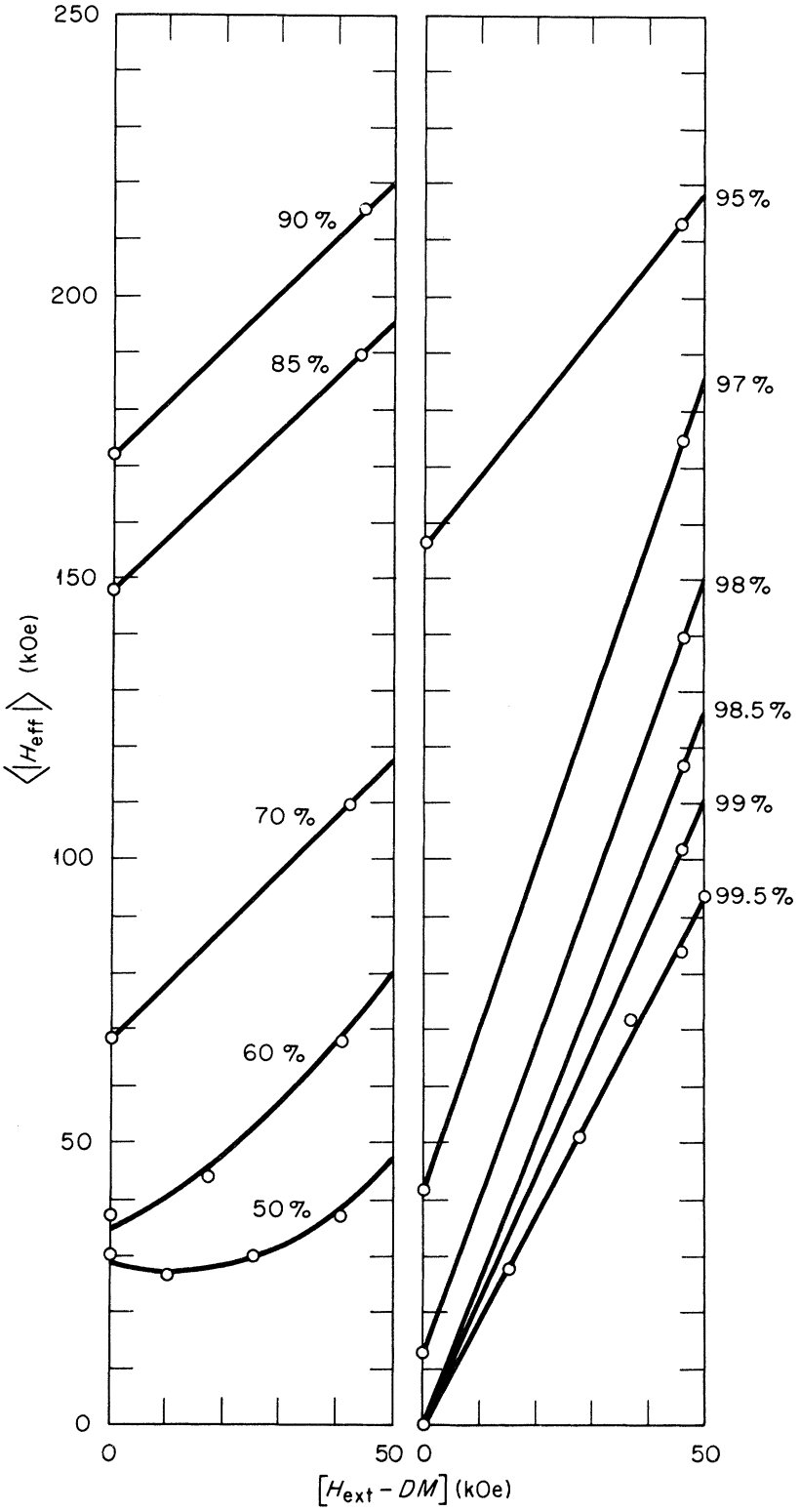

FIG. 4. Experimental values of the effective field at ^{61}Ni nuclei in Ni-Pd alloys (50–99.5% Pd) as a function of external magnetic field. (Percentages given are in at. %.)

from measurements with and without an applied field. Similarly, a measure of the effect of the effect of the distribution can be found from the overlap integral [Eq. (7)]. These calculated values are given in Table III along with the experimental data. In Fig. 6 we plot both $\langle |H_{hf}| \rangle$ and $\langle H_{hf} \rangle$ as a function of Pd concentration. The values obtained for $\langle H_{hf} \rangle_{calc}$ in the mid-concentration range agree

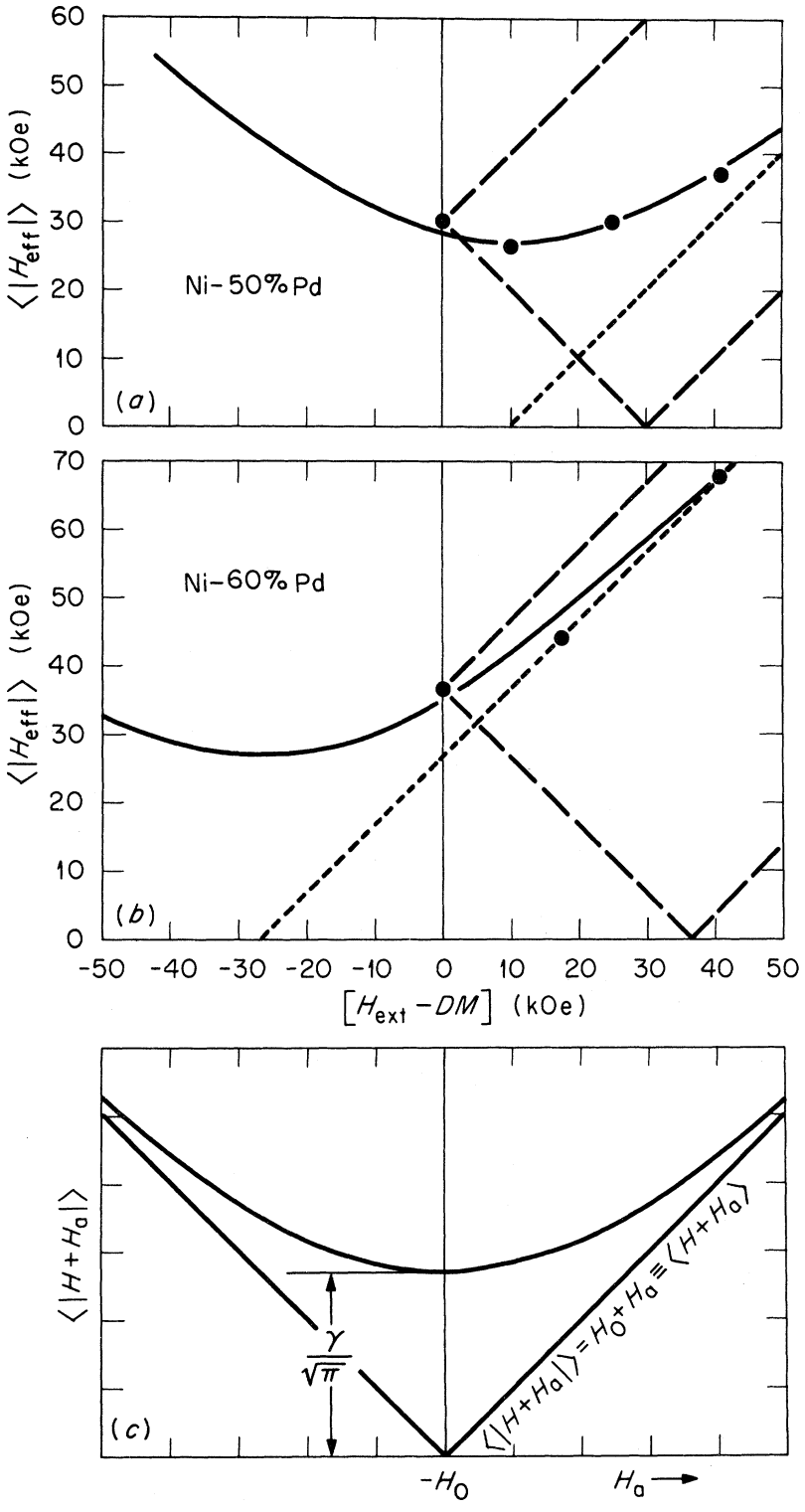

FIG. 5. Behavior of the ^{61}Ni effective field $\langle |H_{eff}| \rangle$ in (a) Ni-50% Pd and (b) Ni-60% Pd as a function of external magnetic field. Solid curves are the theoretical function $\langle |H+H_a| \rangle$ calculated for the values of γ giving the best fit to the data. Dashed lines show the expected behavior of the effective field in the absence of a distribution of fields. The saturation trend of the effective field is illustrated by the dotted lines. (c) Plot of the function

$$\langle |H+H_a| \rangle = (1/\gamma\sqrt{\pi}) \left[\gamma^2 e^{-(H_0+H_a)^2/\gamma^2} + 2(H_0+H_a) \int_0^{H_0+H_a} e^{-B^2/\gamma^2} dB\right].$$

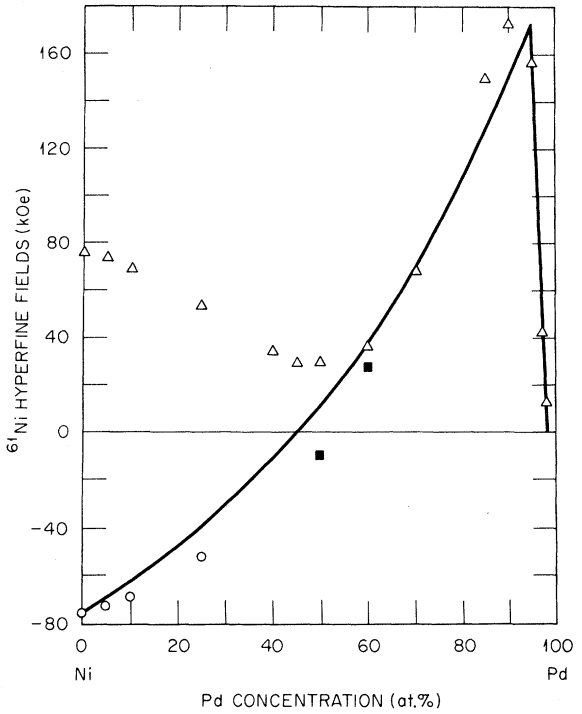

FIG. 6. ^{61}Ni hyperfine fields in Ni-Pd alloys as a function of Pd concentration at 4.2 °K. The average hyperfine fields $\langle H_{hf}\rangle$ (circles) are deduced from the experimental average absolute fields $\langle |H_{hf}| \rangle$ (triangles) and the sign of the field, except in the mid-concentration range where $\langle H_{hf}\rangle_{calc}$ (squares), is calculated with a distribution of fields. The solid line is the theoretical hyperfine field based on a model discussed in the text.

very well with the projected smooth behavior of the field in the region where the overlap integral is small (70-95% Pd), whereas the measured values $\langle |H_{hf}| \rangle$ follow the curvature and trend expected for a distribution of fields. The calculated values of the overlap integral D indicate that it is largest in the mid-concentration range where the centroid of the distribution is passing through the $H=0$ origin. As the hyperfine field begins to increase at higher Pd concentrations, the overlap integral approaches zero and the measured average absolute field approaches the average field, i.e., from Eq. (3),

$$\langle |H| \rangle \to \langle H\rangle \text{ as } D \equiv \int_{-\infty}^{0} H\rho(H)\,dH \to 0 .$$

In order to obtain a measure of the width of the magnetic field distribution, it is necessary to assume an explicit form for the distribution function. In the mid-concentration range a Gaussian distribution would be appropriate if the distribution were caused, for example, by the statistical influence of near-neighbor Pd atoms at a Ni site. Thus, it is assumed

$$\rho(H) = (1/\gamma\sqrt{\pi})\, e^{-(H-H_0)^2/\gamma^2}, \tag{8}$$

where the full width at half-maximum is $\Gamma = \gamma(4\ln 2)^{1/2}$, $H_0 = \int_{-\infty}^{\infty} H\,\rho(H)\,dH$ is the centroid, and $\int_{-\infty}^{\infty} \rho(H)\,dH = 1$. Then for this model, Eqs. (4) and (5) become

$$\langle |H + H_a| \rangle = (1/\gamma\sqrt{\pi})\,[\gamma^2 e^{-(H_0+H_a)^2/\gamma^2} + 2(H_0+H_a)\int_0^{H_0+H_a} e^{-B^2/\gamma^2}\,dB] \tag{9}$$

and

$$M_2(|H+H_a|) = \tfrac{1}{2}\gamma^2 + (H_0+H_a)^2 - \langle |H+H_a| \rangle^2 . \tag{10}$$

The function $\langle |H+H_a| \rangle$ is plotted in Fig. 5(c) below the experimental data for Ni-50% Pd and Ni-60% Pd. When $\Gamma \lesssim |H_0+H_a|$, the curve approaches the limiting value $\langle |H+H_a| \rangle \to (H_0+H_a) \equiv \langle H+H_a\rangle$. The minimum of the function occurs at $(H_0+H_a)=0$, where $\langle |H+H_a| \rangle_{min} = \gamma/\sqrt{\pi}$. Using the definition of γ, this gives for the width of the distribution

$$\Gamma = \langle |H+H_a| \rangle_{min} (4\pi\ln 2)^{1/2} .$$

Comparing Figs. 5(a) and 5(b) with Fig. 5(c) we again note the identifications

$$H = H_{hf}, \quad H_a = H_{ext} - DM, \quad H + H_a = H_{eff}, \quad H_0 = \langle H_{hf}\rangle .$$

Using the values of $\langle H_{hf}\rangle$ from Table III, the solid curves in Figs. 5(a) and 5(b) are the theoretical function $\langle |H+H_a| \rangle$ calculated for values of γ giving the best fit to the data. For Ni-50% Pd and Ni-60% Pd, the distribution widths $\Gamma(50) = (80 \pm 3)$ kOe and $\Gamma(60) = (80 \pm 9)$ kOe are obtained. These values do not give agreement between the experimental second moments $M_2(|H_{eff}|)$ and the theoretical function $M_2(|H+H_a|)$, although the shapes of the two curves are similar. This is perhaps to be expected since $M_2(|H+H_a|)$ is strongly dependent on the functional form of $\rho(H)$. We interpret this to mean that the distribution function $\rho(H)$ is not strictly a Gaussian, but a more strongly peaked function.

For Pd concentrations other than 40-60% Pd, Eq. (1) becomes very nearly an equality and the average field value is obtained from the measured average absolute values and a knowledge of the sign of the field (Fig. 6). The concentration dependence of $\langle H_{hf}\rangle$ can be qualitatively explained by assuming that the hyperfine field is a sum of three terms: (a) a negative contribution from core polarization and the orbital field which is proportional to the local moment on the Ni atom, $a\mu_{Ni}^{d}$; (b) a negative contribution from the bulk conduction electron polarization, $b\bar{\mu}$, where $\bar{\mu}$ is the average magnetic moment of the alloy; and (c) a large positive contribution from Pd neighbors and thus dependent on the local environment of a Ni atom. This term can be thought of as arising from

polarization of the conduction electrons by the Ni magnetic moment, and is written $c\langle n\rangle \mu^d_{\mathrm{Ni}}$, where $\langle n\rangle$ is the average number of Pd atoms in the first coordination shell. Thus, we have

$$H^{\mathrm{Ni}}_{\mathrm{hf}} = a\mu^d_{\mathrm{Ni}} + b\bar{\mu} + c\langle n\rangle \mu^d_{\mathrm{Ni}} . \tag{11}$$

This model is similar to one proposed by Balabanov *et al.*[11] for the Co hyperfine field in Co-Pd. As they pointed out, the large positive contribution to the field in the Pd-rich region cannot be proportional to $\bar{\mu}$, as this would imply that the magnetic moments of the Pd atoms are large, when, in fact, in Ni-Pd the maximum value is $\mu_{\mathrm{Pd}} = (0.25 \pm 0.06) \times \mu_B$ at 71% Pd.[7]

The first two terms in Eq. (11) are found to describe the $3d$ hyperfine fields in many ferromagnetic alloys.[21] In particular, for Ni-based alloys other than Ni-Pd, the values $a = -27$ kOe/μ_B and $b = -93$ kOe/μ_B give good agreement with the experimental values of the hyperfine field. We assume that these contributions to the Ni field from core polarization and bulk conduction-electron polarization are the same in Ni-Pd and that the third term reflects the enhancement properties of Pd. The solid curve in Fig. 6 is the hyperfine field calculated from Eq. (11) with $c = 15$ kOe/μ_B, giving the best fit to the data. Values of $\bar{\mu}$ are taken from saturation magnetization measurements[3,18] and μ^d_{Ni} are taken from the neutron scattering data.[8]

After accounting for effects arising from a distribution of fields, the ^{61}Ni effective field as a function of applied field follows the expected behavior of a ferromagnet up to about 90% Pd (Fig. 4). However, at concentrations greater than about 93% Pd, the increase in slope of the curves reflects the participation of the Pd matrix in a long-range ferromagnetic coupling. The smallest dilution which will support a long-range interaction can be found by estimating the moment associated with Ni impurities in Pd. If the alloy is so dilute that each Ni atom, surrounded by polarized Pd neighbors, can be considered a paramagnetic impurity, then the ^{61}Ni hyperfine field will have an H_{ext}/T dependence given by[22]

$$H_{\mathrm{hf}} = H_{\mathrm{sat}} B_J(\mu H_{\mathrm{ext}}/k_B T) , \tag{12}$$

where B_J is the Brillouin function for spin J, $\mu = g\mu_B J$ is the magnetic moment, g is the atomic g factor, and H_{sat} is the saturation value of the hyperfine field. For H_{ext}/T equal to small values, we have

$$\frac{H_{\mathrm{hf}}}{H_{\mathrm{sat}}} = \frac{(J+1)\mu H_{\mathrm{ext}}}{3J k_B T} . \tag{13}$$

A saturation value can be estimated from Fig. 6 by extrapolating the measured hyperfine field to 100% Pd, giving $H_{\mathrm{sat}} = +225 \pm 25$ kOe. Choosing the applied field data (Fig. 4) of the most dilute alloy studied (0.5% Ni), a plot of $H_{\mathrm{hf}}/H_{\mathrm{sat}}$ vs H_{ext}/T yields a value of $(1.64 \pm 0.10) \times 10^{-2}$ °K/kOe for the slope. From this and Eq. (13), a value $\mu = [J/(J+1)](0.73 \pm 0.05)\mu_B$ is obtained. Since moments of the order $(2-3)\mu_B$ are observed in the concentration range 93–97% Pd,[3,4] we conclude that the magnetic interaction of the Ni impurities with the Pd matrix is strongly concentration dependent. This is in contrast to the giant moments associated with Fe impurities in Pd, where the moments persist at concentrations below the critical concentration.[6]

IV. ENERGY SHIFTS OF THE ^{61}Ni NGR SPECTRA

In Table II the measured absorber recoilless fractions f_A and energy shifts δ_{expt} of the NGR spectra are given. An energy shift of the resonance centroid has contributions from the isomer shift δ_{IS} and the second-order Doppler shift δ_{SOD} and is given by[23]

$$\delta_{\mathrm{expt}} = \delta^A_{\mathrm{IS}} - \delta^S_{\mathrm{IS}} + \delta^A_{\mathrm{SOD}}(T_A) - \delta^S_{\mathrm{SOD}}(T_S) , \tag{14}$$

where the superscripts refer to source and absorber and the temperature dependence of the second-order Doppler shift is indicated. The isomer shift, due to the electric monopole interaction, can be written[24]

$$\delta_{\mathrm{IS}} = K(\Delta R/R)_N \rho_{\mathrm{el}}(0) , \tag{15}$$

where $K = (4\pi c Z e^2/5E_\gamma) R_N^2 = 1.12 \times 10^{-24}$ cm^4/sec for ^{61}Ni, $(\Delta R/R)_N = -(1.2 \pm 0.5) \times 10^{-4}$ is the relative change of the ^{61}Ni nuclear charge radius,[17] and $e\rho_{\mathrm{el}}(0)$ is the electronic charge density at the nucleus calculated from relativistic wave functions. Thus, the change in electronic density at ^{61}Ni in Ni and at ^{61}Ni in Pd can be deduced if the relative second-order Doppler shift is known.

For a nucleus in a pure monatomic lattice, both the second-order Doppler shift and recoilless fraction are given, in the harmonic approximation, by integrals over the phonon frequency distribution $g(\nu)$.[25] In the low- and high-temperature limits the integral can be expanded in terms of the Debye moments ν_n of the frequency distribution, where

$$\nu_n = \left| [(n+3)/3]\, \mu_n \right|^{1/n} , \quad n \neq 0, \quad n > -3$$

and

$$\mu_n = (1/3N) \int_0^\infty \nu^n g(\nu)\, d\nu .$$

At $T = 0$ the expansions become[26]

$$\delta_{\mathrm{SOD}} = -9h\nu_1/16mc \tag{16}$$

and

$$\ln f = -3R/2h\nu_{-1} . \tag{17}$$

For high temperatures we consider only the

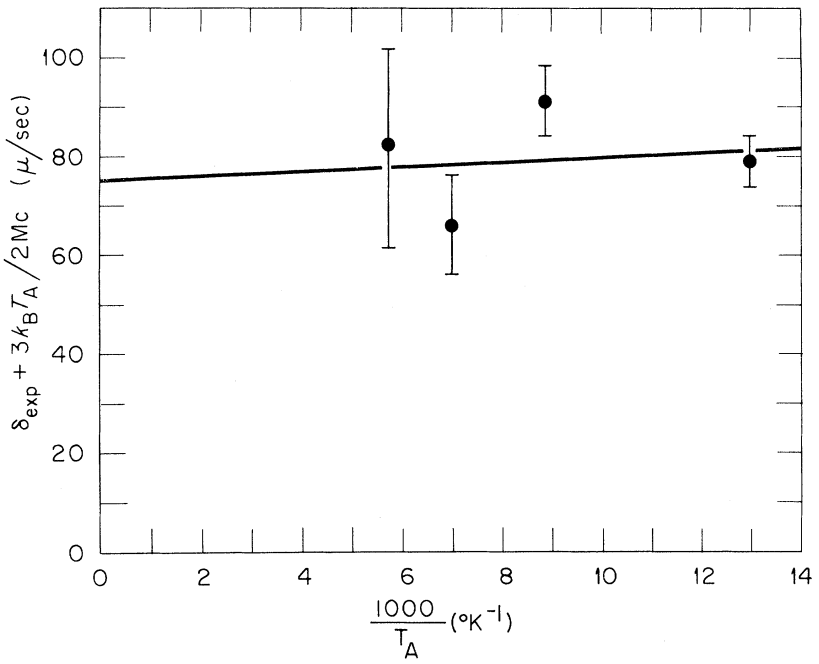

FIG. 7. Temperature dependence of the measured energy shifts for ^{61}Ni as an impurity in Pd, obtained with a Ni-98.5% Pd absorber. The straight line is a linear least-squares fit to the data.

second-order Doppler shift,

$$\delta_{SOD} = (3k_B T/2mc)[1 + \tfrac{1}{20}(h\nu_2/k_B T)^2 + \cdots] \ . \qquad (18)$$

Combining Eqs. (14) and (18), it is seen that a plot of $\delta_{expt} + 3k_B T_A/2mc$ as a function of $1/T_A$ will be a straight line at high temperatures, whose intercept equals $\delta^A_{IS} - \delta^S_{IS} - \delta^S_{SOD}(T_S)$. Figure 7 shows such a plot obtained with a 1.5% ^{61}Ni in Pd absorber and the source maintained at a constant $T_S = 77$ °K. From this plot we obtain

$$\delta^{Pd}_{IS} - \delta^{Ni\text{-}V}_{IS} - \delta^{Ni\text{-}V}_{SOD}(T_S = 77\ ^\circ\text{K}) = +75 \pm 15\ \mu\text{/sec}. \qquad (19)$$

Since the recoilless fraction of the source is $f_s = (16.2 \pm 0.3)\%$ as compared to $f_s = (16.4)\%$ calculated for pure nickel, it is reasonable to assume that δ_{SOD} is the same for the Ni-14% V source and pure Ni. From these observations and from the fact that the energy shift obtained for pure Ni is zero [Table II, Eq. (14)], we conclude that the s electron density at ^{61}Ni in the Ni-14% V source is the same as in pure Ni. Using the calculated value $\delta^{Ni}_{SOD}(T_S = 77\ ^\circ\text{K}) = -98\ \mu$/sec in Eq. (19) gives for the relative isomer shift of ^{61}Ni as an impurity in Pd and in Ni, $\delta^{Pd}_{IS} - \delta^{Ni}_{IS} = -23 \pm 15\ \mu$/sec.

The relative second-order Doppler shift, and hence the relative isomer shift, can be computed directly if the phonon frequency distribution function $g(\nu)$ is known so that δ_{SOD} can be found from Eq. (16). The relative shift follows from Eq. (14) written for two different absorbers using the same source at the temperature:

$$\delta^{Pd}_{expt} - \delta^{Ni}_{expt} = (\delta^{Pd}_{IS} - \delta^{Ni}_{IS}) + (\delta^{Pd}_{SOD} - \delta^{Ni}_{SOD}). \qquad (20)$$

The distribution function $g(\nu)$ has been determined for pure Ni and pure Pd (Refs. 15 and 27, respectively). However, we measure the recoilless fraction for ^{61}Ni as an impurity in these metals and the mass difference and possible force constant changes must be taken into account. In the harmonic approximation, the Debye moments for the impurity scale as

$$\nu_n(\text{imp}) = [M(\text{host})/M(\text{imp})] \times [M(\text{host})/M(\text{imp})]^{1/2}\, \nu_n(\text{host}), \qquad (21)$$

assuming that (a) the host-host and impurity-host spring constants are equal and (b) the mass ratio $M(\text{host})/M(\text{imp})$ is close enough to unity so that localized modes of vibration can be neglected. In Table IV we give the Debye moments calculated from the phonon frequency distribution function $g(\nu)$ and compare the measured recoilless fractions with the theoretical values computed from Eq. (17). The assumptions regarding the scaling of the Debye moments for the ^{61}Ni impurity are certainly true for ^{61}Ni in Ni as can be seen from the agreement between the calculated and experimental recoilless fractions. For ^{61}Ni in Pd the large discrepancy (~ 50%) between the experimental and computed recoilless fraction indicates that the assumptions leading to Eq. (21) are not valid in this case. In particular, localized modes of vibration have been observed by Mozer *et al.*[28] in Ni-Pd alloys containing 5% and 10% Ni using the technique of in-

TABLE IV. Debye moments, recoilless fractions, and energy shifts of ^{61}Ni as an impurity in Ni and in Pd.

		Ni	^{61}Ni in Ni	Pd	^{61}Ni in Pd
Debye moments	ν_{-1}(10^{12} Hz)	8.08	7.93	5.73	7.56
	ν_1 (10^{12} Hz)	8.00	7.85	5.92	7.82
Recoilless fractions	f_{expt}(%)	...	16.0±0.6	...	9.5±1.0[a]
	f_{calc}(%)	...	16.4	...	14.7

Method	$\delta^{Pd}_{SOD}-\delta^{Ni}_{SOD}$ (μ/sec)	$\delta^{Pd}_{expt}-\delta^{Ni}_{expt}$[a] ($\mu$/sec)	$\delta^{Pd}_{IS}-\delta^{Ni}_{IS}$[b] ($\mu$/sec)
(a) Temp. dependence of energy shift	...	...	−23±15
(b) δ_{SOD} from Debye moments	0	+19±7	+19±7
(c) δ_{SOD} from f_{expt} assuming $\nu_{-1}=\nu_1$	+21	+19±7	−2±7

[a]The data for the four absorbers containing 0.5–2.0% Ni were averaged to obtain f_{expt} and δ_{expt} for ^{61}Ni in Pd.
[b]Computed from $\delta^{Pd}_{IS}-\delta^{Ni}_{IS}=(\delta^{Pd}_{expt}-\delta^{Ni}_{expt})-(\delta^{Pd}_{SOD}-\delta^{Ni}_{SOD})$.

elastic neutron scattering. An explanation of the effect upon the recoilless fraction can be found by considering that the light Ni impurities in the heavy Pd host crystal introduce an impurity band above the continuous part of the phonon spectrum. The resulting higher-frequency modes cause a decrease in ν_{-1} from its value in the absence of localized modes and a subsequent decrease in the recoilless fraction.

For the purposes of comparison, Table IV gives the relative isomer shift calculated by three methods: (a) using the temperature dependence of the energy shift, as discussed previously, (b) using Eq. (20) with the relative second-order Doppler shift computed from the Debye moments of the phonon frequency distribution, and (c) using Eq. (20) with $\delta^{Pd}_{SOD}=(178.4/\ln f_{expt})$ μ/sec, which follows from Eqs. (16) and (17) assuming $\nu_1\cong\nu_{-1}$. We expect method (a) to give the correct relative isomer shift, although the statistical error is large due to reduced resonant absorption at higher temperatures. The relative isomer shift as computed with method (b) cannot be considered reliable due to the nonapplicability of the assumptions regarding the scaling of the Debye moment for ^{61}Ni in Pd and the resulting calculation of $\delta^{Pd}_{SOD}-\delta^{Ni}_{SOD}$. The relative isomer shift as calculated by assuming $\nu_1=\nu_{-1}$ for ^{61}Ni in Pd is closer to the more reliable method (a).

Finally, the experimental relative isomer shift is related to the definition Eq. (15):

$$\delta^{Pd}_{IS}-\delta^{Ni}_{IS}=K(\Delta R/R)_N[\rho^{Pd}_{el}(0)-\rho^{Ni}_{el}(0)]=(-23\pm15)\ \mu/\text{sec}.$$

Since $(\Delta R/R)_N$ is negative for ^{61}Ni, this predicts a small increase in the electronic charge density at the ^{61}Ni nucleus in Pd from the charge density at ^{61}Ni in pure Ni.

ACKNOWLEDGMENTS

The authors sincerely appreciate the many helpful suggestions and discussions with J.O. Thomson throughout the course of this work. We thank W. Gläser who actively participated in the early stages of this work. We are also grateful to R. E. Reed and D. E. LaValle for the preparation and analyses of the Ni-Pd alloys.

*Research sponsored by the U. S. AEC under contract with the Union Carbide Corporation.

†Former Oak Ridge Graduate Fellow from the University of Tennessee under appointment with Oak Ridge Associated Universities. Based on a dissertation submitted to the University of Tennessee in partial fulfillment of the requirements for the PhD. degree.

‡Present address: Kernforschungszentrum, Karlsruhe, Germany.

[1]Percentage concentrations are given in at.%.

[2]J. Crangle, Phil. Mag. 5, 335 (1960); R. M. Bozorth, P. A. Wolff, D. D. Davis, V. B. Compton, and J. H. Wernick, Phys. Rev. 122, 1157 (1961).

[3]J. Crangle and W. R. Scott, J. Appl. Phys. 36, 921 (1965).

[4]G. Chouteau, R. Fourneaux, K. Gobrecht, and R. Tournier, Phys. Rev. Letters 29, 193 (1968).

[5]G. G. Low and T. M. Holden, Proc. Phys. Soc. (London) 89, 119 (1966); A. T. Aldred, B. D. Rainford, and M. W. Stringfellow, Phys. Rev. Letters 24, 897 (1970).

[6]P. P. Craig, D. E. Nagle, W. A. Steyert, and R. D. Taylor, Phys. Rev. Letters 9, 12 (1962).

[7]J. W. Cable, E. O. Wollan, and C. W. Koehler, Phys. Rev. 138, A755 (1965).

[8]J. W. Cable and H. R. Child, Phys. Rev. B 1, 3809 (1970).

[9]*Hyperfine Structure and Nuclear Radiations*, edited by E. Matthias and D. A. Shirley (North-Holland, Amsterdam, 1968).

[10]P. P. Craig, B. Mozer, and R. Segnan, Phys. Rev. Letters 14, 895 (1965).

[11]A. E. Balabanov, N. N. Delyagin, A. L. Yerzinkyan, V. P. Parfenova, and V. S. Shpinel, Zh. Eksperim. i Teor. Fiz. 55, 2136 (1968) [Sov. Phys. JETP 28, 1131 (1969)]; P. Reivari, Phys. Rev. Letters 22, 167 (1969).

[12]F. E. Obenshain, W. A. Gläser, G. Czjzek, and J. E. Tansil, J. Phys. Radium 32, 783 (1971); in *Hyperfine Interactions in Excited Nuclei*, edited by G. Goldring and R. Kalish (Gordon and Breach, New York, 1971), Vol. 3, p. 846.

[13]U. Erich, J. Göring, S. Hüfner, and E. Kankeleit, Phys. Letters 31A, 492 (1970).

[14]R. E. Watson and A. J. Freeman, Phys. Rev. 123, 2027 (1961); A. J. Freeman and R. E. Watson, in *Magnetism*, edited by G. T. Rado and H. Suhl (Academic, New York, 1965), Vol. IIA, pp. 168ff.; R. E. Watson, in *Hyperfine Interactions*, edited by A. J. Freeman and R. Frankel (Academic, New York, 1967).

[15]R. J. Birgeneau, J. Cordes, G. Dolling, and A. D. B. Woods, Phys. Rev. 136, A1359 (1964).

[16]E. N. Shipley, R. E. Holland, and F. J. Lynch,

Phys. Rev. 182, 1165 (1969).
[17]J. C. Love, F. E. Obenshain, and G. Czjzek, Phys. Rev. B 3, 2827 (1971).
[18]G. Fischer, A. Herr, and A. J. P. Meyer, J. Appl. Phys. 39, 545 (1968).
[19]J. W. Burton, in Oak Ridge National Laboratory Report N ORNL-4743 (unpublished).
[20]H. H . Wegener and F. E. Obenshain, Z. Physik 163, 17 1).
[21]D. A. Shirley, S. S. Rosenblum, and E. Matthias, Phys. Rev. 170, 363 (1968).
[22]C. Kittel, *Introduction to Solid State Physics* (Wiley, New York, 1967), p. 435.
[23]A. A. Maradudin, in *Solid State Physics*, Vol. 18, edited by F. Seitz and D. Turnbull (Academic, New York, 1966), p. 389.
[24]A. J. F. Boyle and H. E. Hall, Rept. Progr. Phys. 25, 441 (1962).
[25]H. H. F. Wegener, *Der Mössbauer Effekt* (Bibliographisches Institut, Mannheim, 1965), pp. 61 and 109.
[26]R. M. Housley and F. Hess, Phys. Rev. 146, 517 (1966).
[27]A. P. Miller and B. N. Brockhouse, Can. J. Phys. 49, 704 (1971); and A. P. Miller (private communication).
[28]B. Mozer, K. Otnes, and V. W. Myers, Phys. Rev. Letters 8, 278 (1962).

PHYSICAL REVIEW B VOLUME 6, NUMBER 7 1 OCTOBER 1972

Spatially Random Heisenberg Spins at Very Low Temperatures. I. Dilute Ferromagnet*

Raza A. Tahir-Kheli
Department of Physics, Temple University, Philadelphia, Pennsylvania 19122
(Received 24 January 1972)

A formulation is given for calculating magnetic-single-site density of states for a completely random dilute Heisenberg ferromagnet, with isotropic nearest-neighbor exchange, in the limit of very low temperatures. In conformity with Kohn's suggestion that the dynamics of sufficiently random many-body systems may be approximated by that of typical small neighborhoods, a consistent hierarchy of truncation schemes for the spatial matrix elements of the T matrix is described. The case of a drastically truncated Kohn neighborhood, consisting only of two neighboring sites, is worked out in detail. It is shown that for lattices without nearest-neighbor triangles, the given density of states exactly preserves the first four frequency moments. Moreover, for Bravais lattices with z nearest neighbors, all frequency moments of the density of states are given exactly to the two leading orders in z^{-1}. By analyzing the renormalization of the $K \to 0$ spin-wave energy, estimates for the critical temperature are obtained. In the present approximation, the magnetic long-range order cannot occur for magnetic concentrations which are $\leq 2/z$. For the simple-cubic lattice, numerical computations of the magnetic-single-site density of states and the real and imaginary parts of the coherent exchange are given for several concentrations.

I. INTRODUCTION

The ground state of a dense Heisenberg ferromagnet is exactly known. However, as soon as finite concentrations of nonmagnetic impurities are introduced, the system becomes a random coupled many-body system which cannot be solved exactly in arbitrary dimensionality. Brout[1] seems to have been the first one to seriously address himself to the question of the behavior of such a dilute Heisenberg ferromagnet as a function of the dilution. His analysis was rather formal, and although no precise results were recorded, a qualitative picture of the dependence of the Curie temperature $T_C(m)$ as a function of the magnetic concentration m was predicted. In the limit that the exchange interactions are extremely long ranged, the dependence of $T_C(m)$ on m was conjectured to be linear. For finite-range interactions, the linear dependence was conjectured to be confined to the concentrated region, while in the vicinity of a certain nonzero critical concentration m_c [m_c is the highest relative concentration of magnetic ions for which magnetic long-range order (LRO) does not occur] the behavior was expected to be more complicated.

The problem was later studied by Elliott[2] and Smart.[3] Elliott[2] used the constant-coupling two-particle cluster approximation of Kasteleijn and van Kranendonk.[4] For spin S and coordination number z, he estimated the critical concentration m_c as

$$m_c = (S+1)/S(z-1) . \tag{1.1}$$

Smart[3] generalized the Bethe-Peierls-Weiss method for application to the classical spin[5] case (i.e., $S \to \infty$) and found the same result.

Charap[6] argued that because of the neglect of concentration fluctuations in the environment of the nearest-neighbor shell, the physics of the problem had been inadequately represented in this[3] treat-